EEET ECOLOGICAL ENGINEERING & ENVIRONMENTAL TECHNOLOGY

Ecological Engineering & Environmental Technology 2024, 25(7), 118–132
https://doi.org/10.12912/27197050/188191
ISSN 2719-7050, License CC-BY 4.0

Received: 2024.04.22
Accepted: 2024.05.06
Published: 2024.06.01

Applying Remotely Sensed Imagery to Extract Geological Lineaments South Rifian Ridges, Morocco

Mohammed El Aoufir[1*], Mohamed Benabbou[1], Brahim Benzougagh[2], Slimane Sassioui[3], Hicham El Asmi[1], Abdelfattah Elkourchia[4], Mustapha Elabouyi[4]

[1] Laboratory of Geosciences, Environment, and Associated Resources (LGERA), Faculty of Sciences Dhar Mehraz, Sidi Mohamed Ben Abdellah University, Fez-Morocco

[2] Geophysics and Natural Hazards Laboratory, Scientific Institute; Geophysics, Natural Patrimony and Green Chemistry Research Center "GEOPAC", Mohammed-V University in Rabat, Avenue Ibn Battouta, P.B 703, 10106 Rabat-City, Morocco

[3] Laboratory of Analysis and Modelling of Water and Natural Resources, Mohammadia School of Engineers, Mohammed V University in Rabat, Morocco

[4] Department of Geology, Faculty of Science, Moulay Ismail University, Meknes, Morocco

* Corresponding author's e-mail: mohammedelaoufir2@gmail.com

ABSTRACT

The South Rifain ridges are an example of tectonic-sedimentation interaction in the Mio-Plio-Quaternary foreland basins at the front of the Rif chain. is an elongated mountain zone-oriented E-W and N-S, forming the most frontal part of the Rif belt. The morphotectonic study carried out in this area is based on Landsat-8 OLI image processing techniques to determine the contribution of these images to structural mapping. The results obtained reveal a predominant E-W orientation, which is widely present throughout the study area. This is followed by a second N-S direction, a third NW-SE direction, and a fourth NE-SW direction. The NW-SE lineaments are also mapped in kilometres. Their equivalent on the ground shows a sinister movement but does not show a significant horizontal displacement of more than a few metres. Together with the NE-SW faults, these faults form a conjugate system of dextral and sinistral faults, compatible with a palaeostress field where the maximum shortening stress is submeridian.

Keywords: South Rifain Ridges (Morocco); Landsat-8; geological lineaments; structural mapping.

INTRODUCTION

Geological lineaments, which include fault systems, fractures, and linear structures, are important parts of the Earth's surface and play an essential role in geological studies, particularly in geological processes, tectonic history, and the potential for natural resources [Masoud and Koike, 2006; Adiri et al., 2017; Doski, 2019; Ahmadi et al., 2023]. These lineaments provide a rare window into the inner workings of the Earth and important hints about the forces that have produced and are still shaping our globe. For instance, the investigation of fault systems reveals the intricate interactions of tectonic plates, revealing seismic activity and earthquake potential in various parts of the world. Similar geological events, such as the creation of mineral deposits, groundwater flow patterns, and the evolution of landscapes, are revealed by the investigation of fractures and linear structures [Preeja K. R. et al., 2011; Dang et al., 2018].

Traditionally, Intensive fieldwork and manual mapping methods, which frequently encountered problems in distant or difficult terrains, were required for the identification and characterization of these structures [Stead et al., 2019]. However, an innovative era in geological studies has begun with the development of remote sensing technology, which provides a more effective, affordable,

and precise method of identifying and evaluating geological lineaments [Das et al., 2009; Ahmed Ii and Mansor, 2018; Chaves et al., 2020; El Hafyani et al., 2023].

Given its ability to provide very interesting information, due to high spatial resolution images, remote sensing has become common and more usable in geological research, even in geographically difficult environments. In Morocco, this technique has been widely used in geological studies, especially in geological mapping and structural analysis [Zafaty et al., 2023], mining prospecting [Benaissi et al., 2022], mapping of hydrothermal alteration zones [Mamouch et al., 2022], and automatic lineaments extraction [Adiri et al., 2017; Jellouli et al., 2021; Si Mhamdi et al., 2017].

This study, focus on the South Rifian Ridges (SRR) region in Morocco, renowned for its complex geological history and the presence of potentially significant geological lineament-related features. The SRR area presents a unique geological setting that has garnered interest due to its distinct topographic characteristics and geological phenomena [Faugères, 1978; Ait Brahim et al., 1984; Haddaoui et al.,1997; Amine et al., 2020]. The aim of this paper is to demonstrate the effectiveness of remote sensing data in the extraction and analysis of geological lineaments in the SRR of Morocco. By adopting advanced image processing and automated algorithms, the lineaments have been identified by highlighting the geological evolution of the area.

MATERIALS AND METHODOLOGY

Study area

The study was conducted at the south front of the Rif belt, at the boundary between the Saiss basin to the south and the Gharb basin to the west. This area, which forms part of the southern front of the Rif belt, has a relatively clearly marked structure compared with the Rif belt [Chalouan et al., 2003 ; Amine et al., 2020; El Asmi et al., 2023a; El Asmi et al., 2023b; Taj et al., 2024; El Yakouti et al., 2024]. The SRR form the front of the Rif belt, of which they constitute the foreland at the boundary between two very different structural domains: the Rif to the north, an alpine mountain belt formed between the Triassic and Upper Miocene, and the Meso-Atlas domain to the south, with a Palaeozoic basement structured by Hercynian tectonics, and a very thick and relatively undeformed Mesozoic cover (Fig. 1). The Ridges are subdivided into two major groups: a western group that arches and curves westward (Jbel Kefs, Jbel Outita, and Jbel Bou Draa), and an eastern group that forms a less pronounced arc (Jbel Kannoufa, Jbel Zerhoun, and Jbel Dhar N'Sour), (Fig. 2). Further to the east, in the extension of the second group, two other isolated small ridges can be found: Jbel Trhat and Jbel Zalarh [Faugères, 1978; Haddaoui, 1997].

The primary structuring of the South Rif Ridges occurred during the upper Miocene due

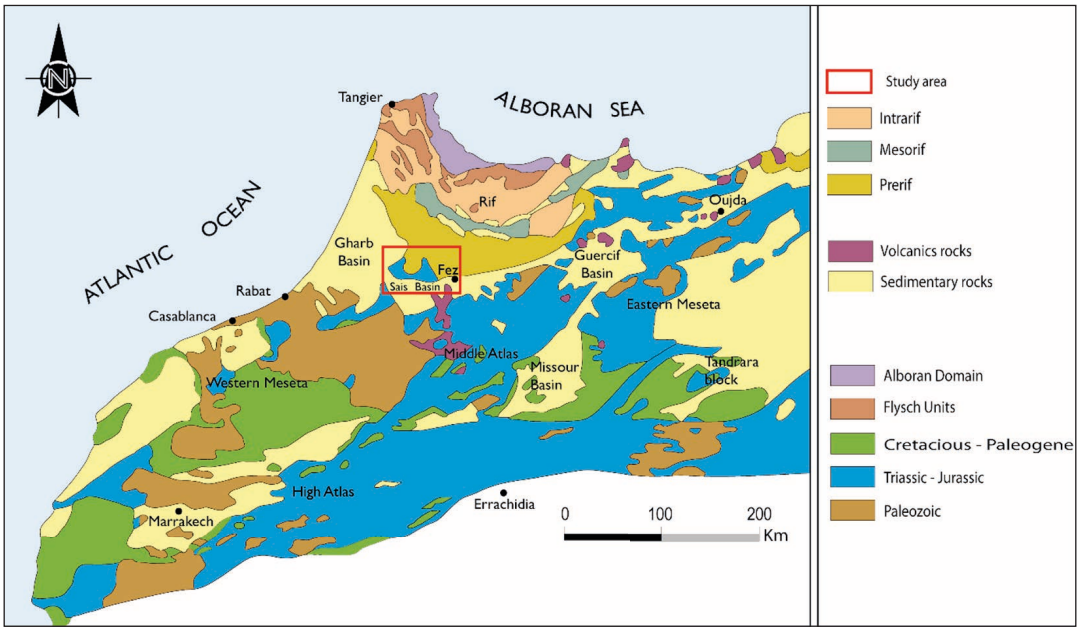

Fig. 1. Geographic and geological context of study area [Frizon de Lamotte et al., 2008]

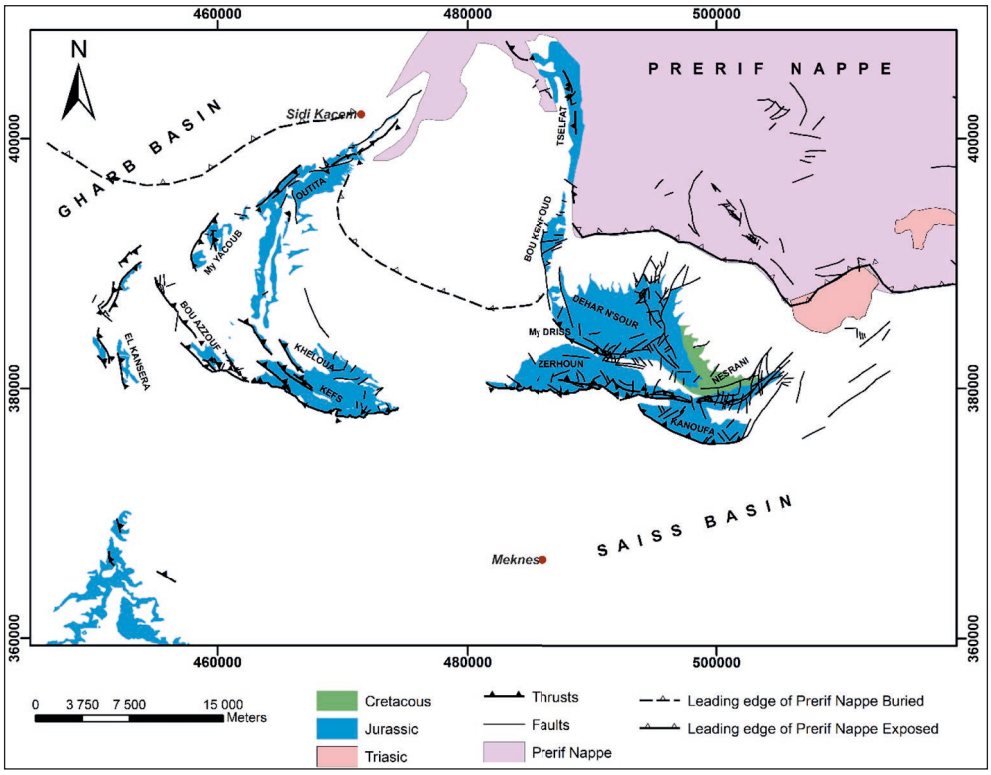

Fig. 2. Geological map of the South Rifain Ridges [Faugères, 1978]

to the advancement of the external Rif (Pre-Rif) from the east-northeast towards the west-southwest [Faugères, 1978]. From a stratigraphic level, the South Rif Ridges are characterized by a highly diverse Jurassic sedimentary sequence. Faugères (1978) divided the sedimentary sequences into three units: (i) Peripheral Units: These units have sedimentary sequences that do not exceed the Middle Lias. This type characterizes the El Kansera, Tekerma, Kannoufa, Moussoua, Nesrani, and Oued Beht ridges. (ii) Intermediate Units: These units are characterized by deposits of carbonate internal platform from the Lower and Middle Lias, overlain by an incomplete series of the Upper Lias to Bajocian. The Kefs, Moulay Yacoub El Hamma, Outita, Jbel Nouella, Jbel Balaàs, and Koudia Bou Azzouf ridges belong to this lithostratigraphic category. (iii) Central Units: They exhibit significant thicknesses of marly and marl-limestone facies from the Toarcian and Bajocian. The Dhar-En-Nsour, Zerhoun, Fert-El-Bir, Tselfat, Trhat, and Zalarh ridges fall within this lithostratigraphic category (Fig. 3).

Adapted methodology

The Landsat Operational Land Imager (OLI) image of August 5, 2020, downloaded from the United States Geological Survey website (https://earthexplorer.usgs.gov) has been used in this work to map and extract the lineaments. After the radiometric calibration and the atmospheric correction, a panoply of processes has been applied which are: color composition, band ratio, principal component analysis (PCA), and directional filters. Then, the extracted lineaments have been validated using geological map and field data (Fig. 4).

In Morocco, several studies were carried out using remote sensing. [Adiri et al., 2017; Hamidi et al., 2023] conducted a study with the aim to compare the different remotely sensed data in automatic lineaments extraction such us: ASTER, Landsat 8 and Sentinel. The validation of the different results derived from this work showed that the sentinel 1 are the most efficient data in the restitution of the lineaments. In Kerdous inlier of the Anti-Atlas belt, Morocco, [Jellouli et al., 2021] carried out a study with the objective of the lineaments mapping using optical and radar remote sensing data. The validation of the results using geological map of the region and ground truth showed that HH and HV polarizations of ALOS POLSAR and PC1 of Landsat data are more efficient in lineaments mapping. In 2022, a study carried out by [Benaissi et al., 2022] in the Aouli inlier (Eastern Meseta, Morocco).

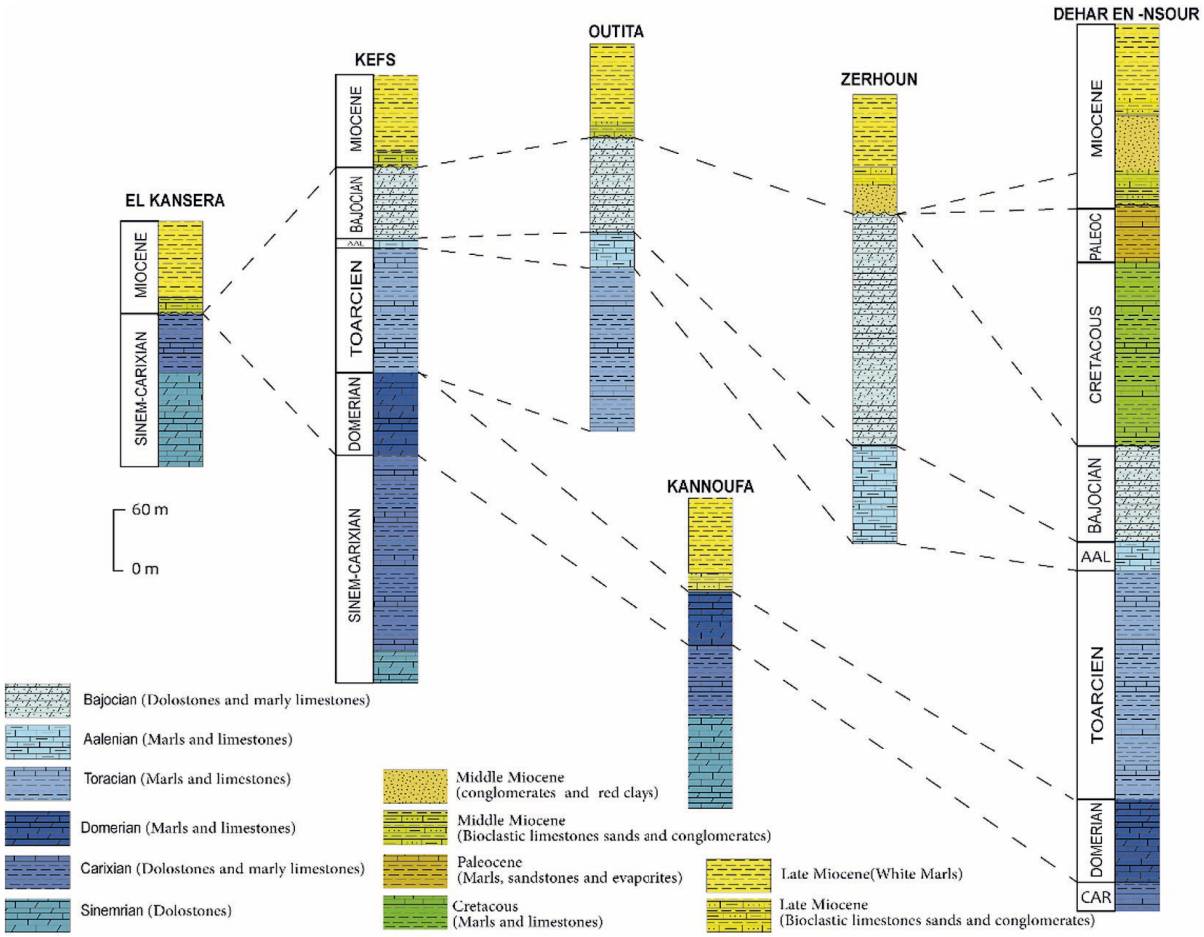

Fig. 3. Series and lithostratigraphic correlations in the South-Rifian Ridges modified from [Haddaoui et al., 1997]

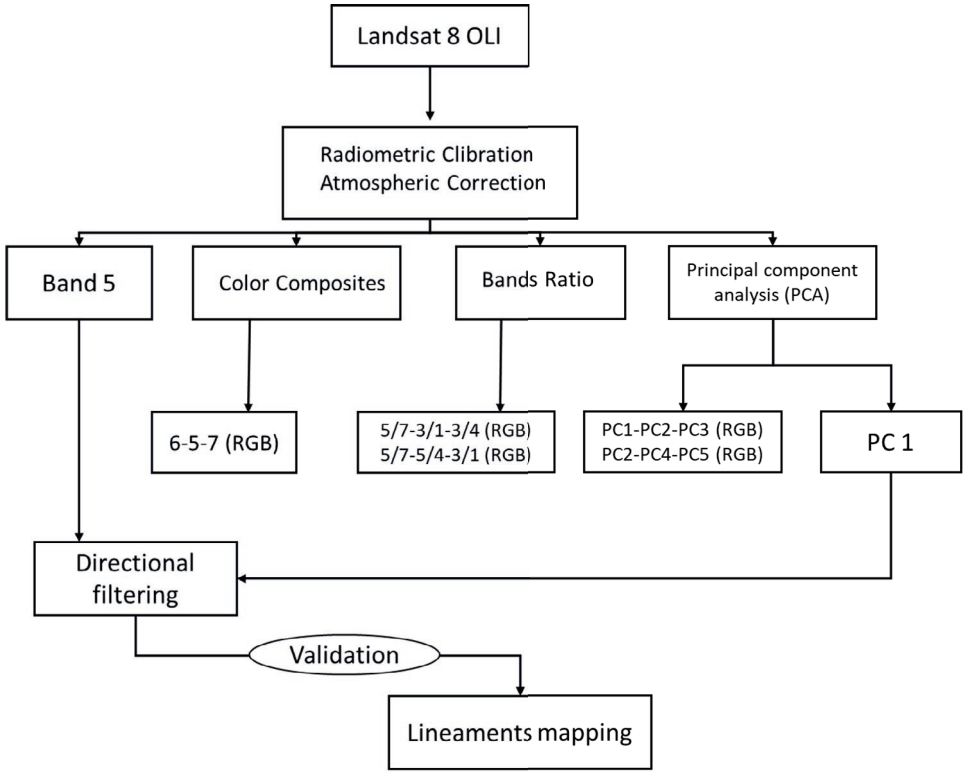

Fig. 4. The flowchart of the data sources and methodology

Radiometric calibration and atmospheric correction

There has been a considerable amount of research carried out into the effects of atmospheric scattering on remote sensed data. This stage, which has an important role in the identification of the pixel content. Several algorithms ca be found in the literature in this sense such as: FLAASH (Fast Line-of-sight Atmospheric Analysis of Spectral Hypercubes) developed for the first time in MODTRAN (MODerate resolution atmospheric TRANsmission) [Anderson et al., 2012], and dark object subtraction (DOS) [Chavez, 1988] that has been used in this study for atmospheric scattering of Landsat data. This algorithm starts always with the assumption that there are some pixels in the image which must have a 0% in reflectance value.

Color composites

The RGB color composites method was used to create colored images that reflect the spectral characteristics of the spatial data [Abrams et al., 1983; Sassioui et al., 2023]. In Table 1, various combinations are presented, tailored for geological surveys.

Band ratios

This remote sensing method is widely used in geological studies [Amer et al., 2010; Ali et Pour, 2014; Yousefi et al., 2018]. The concept of band ratios involves a transformation in which the numerical value of one band is divided by that of another band [Mars and Rowan, 2010; Pour and Hashim, 2012]. The choice of bands for establishing these ratios depends on the reflection and absorption properties of a specific target [Amer et al., 2010].

Principal component analysis (PCA)

Principal Component Analysis (PCA), which is also utilized for lineament extraction, enables the examination of variability and dispersion in data from several spectral bands [Fossi et al., 2021; Khan et al., 2023]. It is a geometric model-based descriptive approach. PCA is used to create a new image where the bands are not connected with each other because spectral bands are frequently related to one another [Ortiz et al., 2019; Islam et al., 2023]. The main application of this technique is to produce color composites of the first three elements. These are great for visual interpretation since they increase the contrast between different ground features.

RESULT AND DISCUSSION

Colors composites

A number of spectral sign combinations were evaluated during processing; in reality, the blue band, the infrared band (NIR), and the mid-infrared 2 (SWIR2) in RGB (RGB: 257) provide the greatest result and contain the most information according to the optimal factor index (OIF). The RGB color composites revealed a limited level of information regarding the delineation of lithological units, despite visually exploring several combinations of RGB bands. This limitation can be partially attributed to the extent of the study area. However, in-depth observations demonstrated that the use of bands 6, 5, and 7 allowed for a clear distinction between the Quaternary formation and other geological formations in our study region (Fig. 5). These geological interpretations represented the Quaternary Formation in green, which is predominant in a significant area. To enhance our analysis, we also employed (PCA) and the use of band ratios. Based on reflectance characteristics, the RGB color composite resulting from the PCA

Table 1. Color compositions of Landsat 8 bands used in geological exploration [Lilleasnd et al, 1987]

Colors composites (RVB)	Characteristics
4-3-2	Real color of the image.
2-4-6	Interesting to discern the lithological limits between rocks.
7-6-5	Best result to use for geological analysis, band 5 is concerned with the presence of iron, band 6 characterizes the general albedo of materials and band 7 is that of hydroxyl minerals.
7-5-2	Provided the minimum data redundancy, the best result to differentiate between different rock units.

results (PC2, PC4, and PC5) revealed significant distinctions in the reflectance of different lithological units (Fig. 6). This visual representation distinguished the Quaternary formations in blue, Jurassic limestone formations in purple, Pliocene and Miocene formations in pink, while urban areas, i.e., areas inhabited by humans, were highlighted in turquoise.

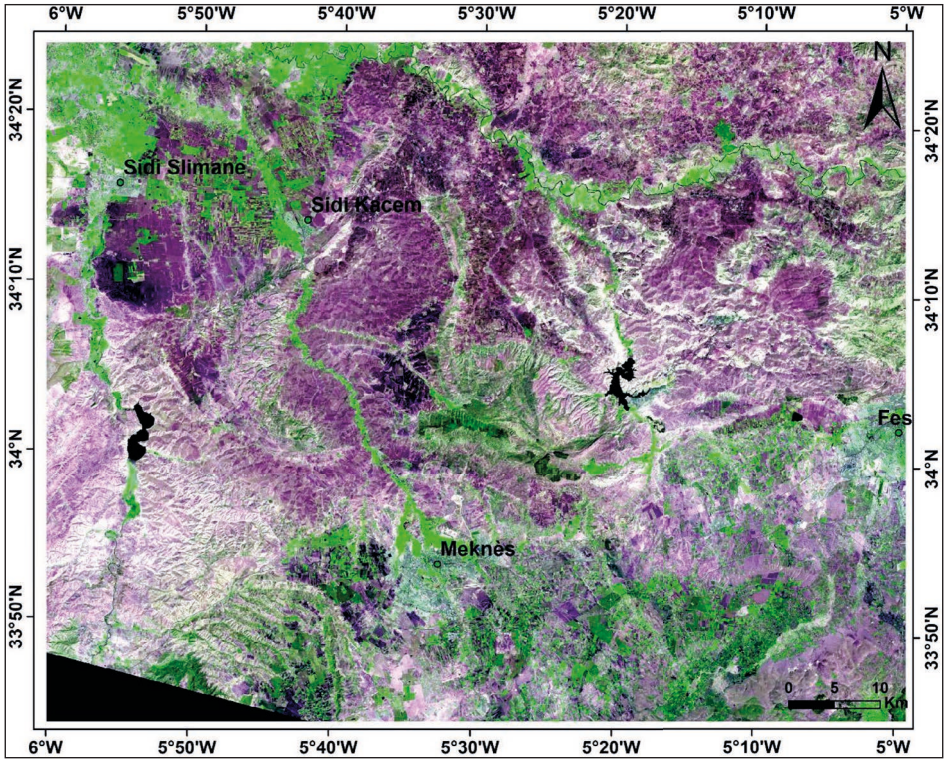

Fig. 5. RGB color composite image (Band 6, Band 5, and Band 7 in RGB)

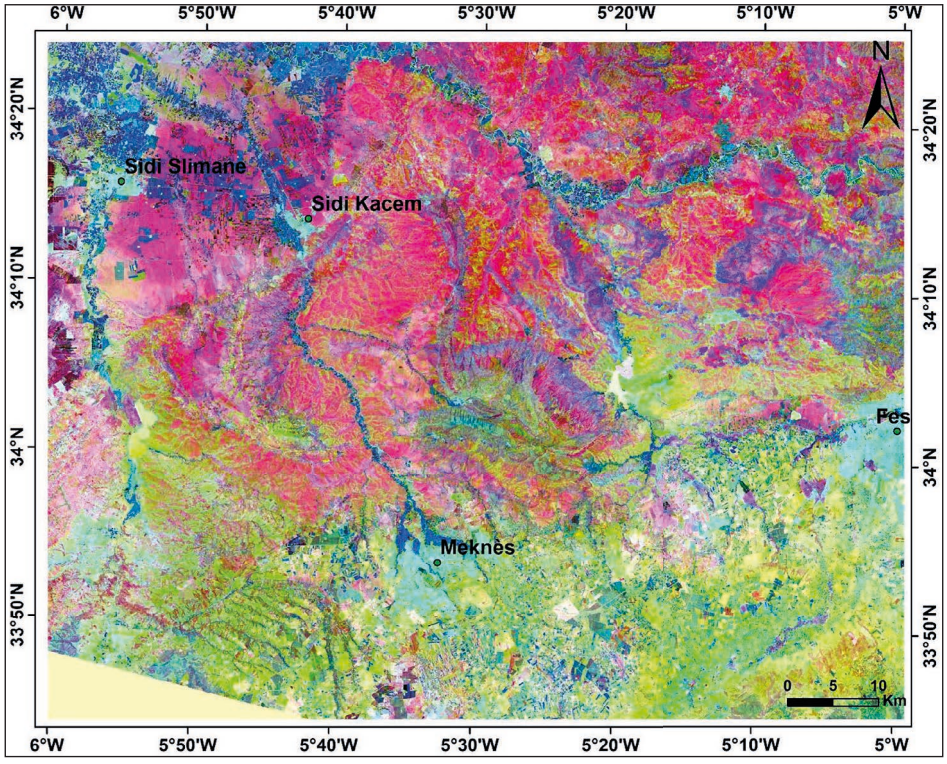

Fig. 6. RGB color composite image (PC2, PC4, and PC5 in RGB)

Band ratios

In terms of band ratios, the high iron oxide content of sandstone a characteristic that has been extensively studied by [Ali and Pour, 2014] proved to make the 4/5 ratio especially useful for sandstone discrimination. Additionally, because of their high iron oxide content, shales and clays that are rich in mica and clay minerals can be distinguished using the 7/5 ratio [Harris et al., 2005]. Studies by [Mahan and Arfania, 2018] further show that the 3/2 band ratio can be effectively used to determine the presence of iron oxides in rocks. The data of study area, indicate that the RGB composites obtained from the 7/5, 3/2, and 4/5 band ratios were favored because of the striking contrast they offer between various rock units (Fig. 7). The cerulean blue representation of the Miocene and Pliocene formations is noteworthy. The vast sand formation that occupied a large part of the landscape were depicted in green, while the Jurassic structures were emphasized in dark yellow.

Mapping of lineaments

Applying directed filters to the first seven principal components (PCA) and all seven bands from 1 to 7 is the automatic lineament extraction method. In order to ensure that all pertinent lineaments are taken into account, this technique attempts to thoroughly cover all conceivable orientations of lineaments in the study region. To extract lineaments from each band and the primary components of PCA, a comprehensive analysis was carried out. Following a thorough analysis, the best results were found using bands 5 and PCA 1 (Fig. 8 and 9).

Figure 9 shows the synthetic lineament map that was created for the research region by combining data from the lineament maps of band 5 and PCA 1. Nevertheless, in order to exclude unwanted linear features like highways, rivers, and mountains, this map has to be corrected. To achieve an accurate depiction, it is also necessary to correct the geometry of lineaments and remove duplication.

Google Earth images were used for verification, and the results were compared to previously collected data to see how accurate the results were. The density map that was created (Fig. 11), places high density values in regions with competent lithological units and the majority of low values (mid to low densities) in regions with less resistant lithological units. This knowledge aids in a more accurate assessment of the data and is useful for comprehending the distribution of geological features in the studied area.

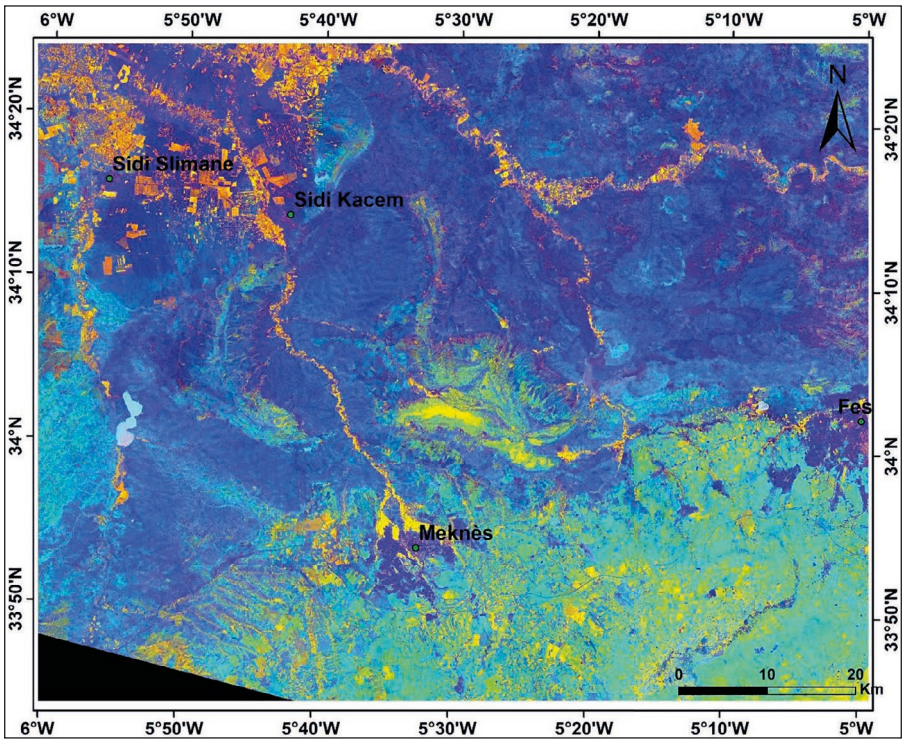

Fig. 7. RGB color composites of 7/5, 6/4, and 4/2 as band ratio-derived images

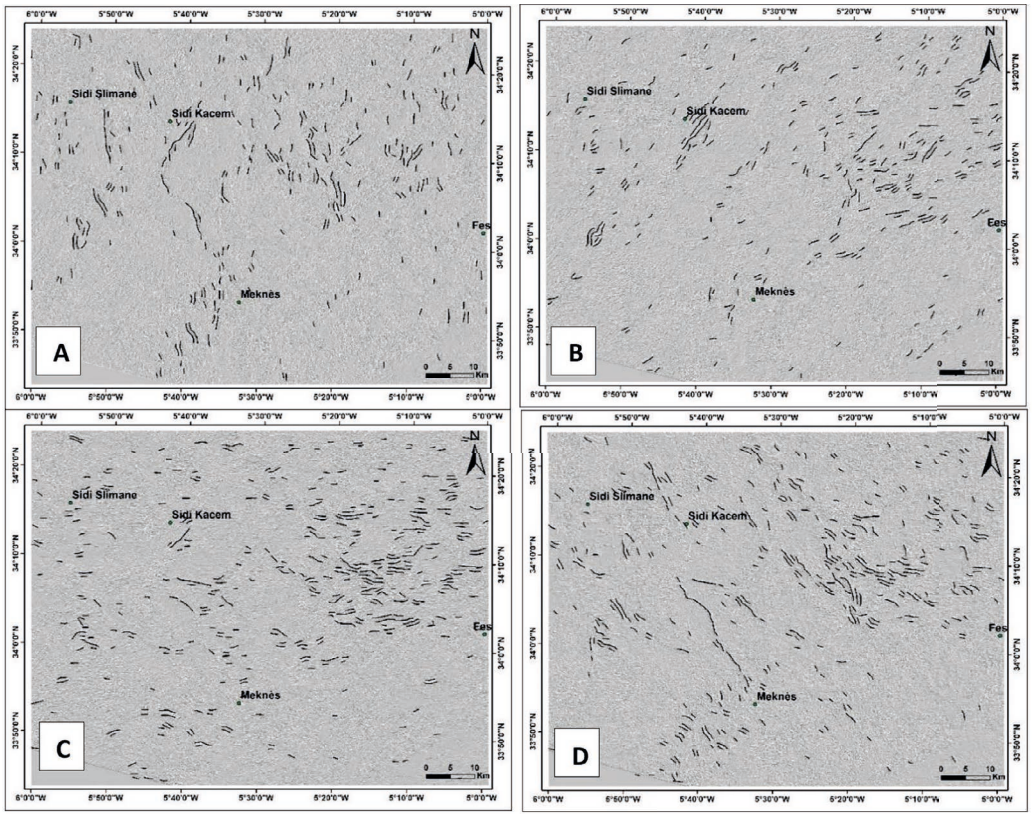

Fig. 8. Lineaments extracted from the spatial filtering of Landsat 8 OLI Band 5 (B5); (a) N-S Filter, (b) NE-SW Filter, (c) E-W Filter, (d) NW-SE Filter

The lineament map obtained in this area reveals two families of faults, transverse and longitudinal to the Jurassic ridges (Fig.11). These lineament traces are then represented as a rosette (Fig. 12), They can be divided in four principal directions: The E-W lineaments (N75°E–N110°E) are organised into bands forming the axes of the Jurassic anticlinal ridges in the sector. Four bands of multi-kilometre length can be distinguished Moulay Idriss-Fert el Bir, Jbel Zerhoun-Jbel Nesrani, Jbel Tekerma-Jbel Kannoufa, and Jbel Kefs (Fig.2). In the field, faults in this direction

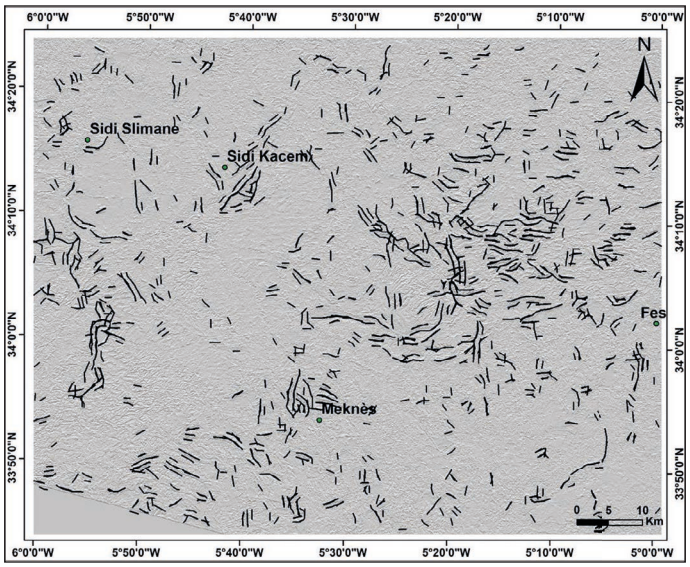

Fig. 9. Lineaments extracted from the spatial filtering of Landsat 8 OLI PC1 in the four directions: N-S, NE-SW, E-W, and NW-SE

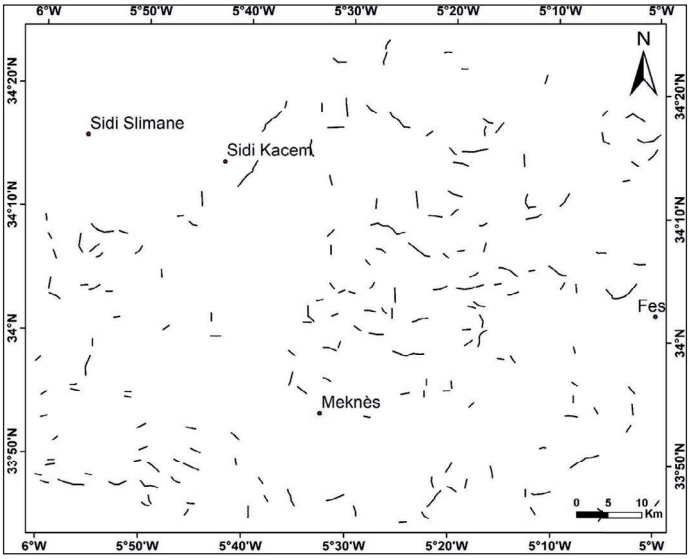

Fig. 10. Synthetic lineament map of PC1 and band 5 in the study area

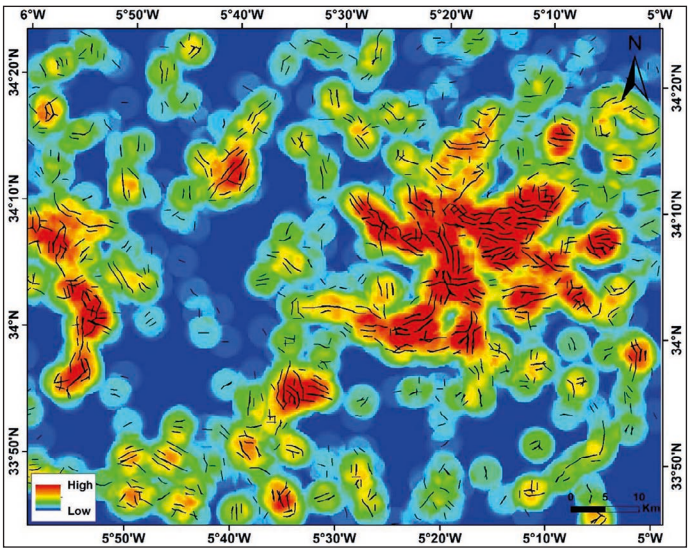

Fig. 11. Lineament density map of study area

correspond to reverse or thrust faults towards the south and are responsible for the edification of Jurassic anticlinal ridges. [Faugères, 1978; Haddaoui et al., 1997; Sani et al., 2007; Amine et al., 2020]. In Jbel Zerhoun-jbel Nesrani they are marked by Triassic injection at the north of jbel Tekerma, thus indicating the role of Triassic clays in initiating the E-W decollement [Zizi, 2002]. The direction of these sub-equatorial lineament's changes in the area at the edge of the study area. Thus, the Moulay Idriss-Fert el Bir E-W line, while along the axis of the associated ridge, progressively turns NW-SE (N126°E) towards the west as it approaches the Volubilis submeridian corridor. Similarly, the Jbel Zerhoun-Jbel Nesrani line progressively turns NE-SW (N45°E) towards the east, where, outside the study area, a major NE-SW fault limits South Rifain ridges to the east.

The NE-SW lineaments (N35°E–N75°E) are distributed along the sector studied, with a relatively clear concentration at Moulay Idriss. They can be mapped over several kilometres. On the field, these are sinistral faults. To the east a group of faults oriented globally NE-SW (N50), constituting the major Moulay Yacoub corridors, which appear to have an important role in secondary and tertiary palaeogeography and from there impacting the general structure of the South Rifain ridges [Faugères, 1978; Haddaoui et al., 1997; Sani et al., 2007].

The NW-SE lineaments (N120°E–N145°E) also present a kilometre-scale map. Their equivalent in the field presents a dextral displacement but does not seem to have a significant horizontal displacement, which does not exceed a few metres. These faults, combined with the NE-SW faults, form a conjugate system of dextral and sinistral faults, which are consistent with a paleostress reconstruction where the maximum shortening stress is submeridian [Bargach et al., 2004; Chalouan et al., 2014].

The NNW-SSE to NNE-SSW lineaments (N170°E–N30°E) are represented in the sector studied, with the Moulay Idriss and Zerhoun ridges to the west and the Jbel Nesrani and Kannoufa ridges to the east [Chalouan et al., 2014]. In fact, they are organised into two corridors that cut through the secondary and tertiary (Neogene)

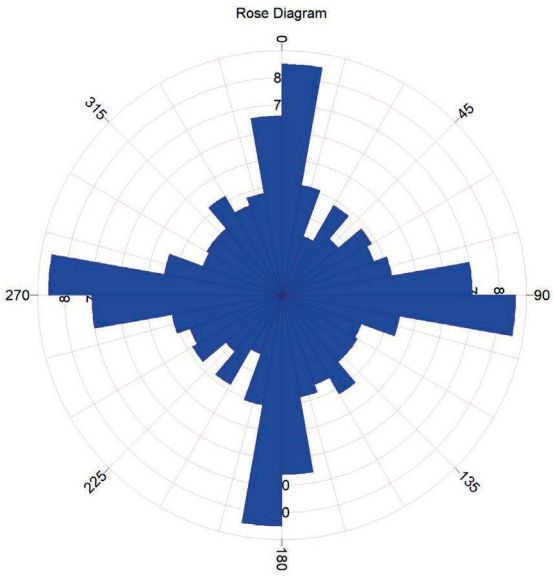

Fig. 12. Rosette of lineament orientations of study area

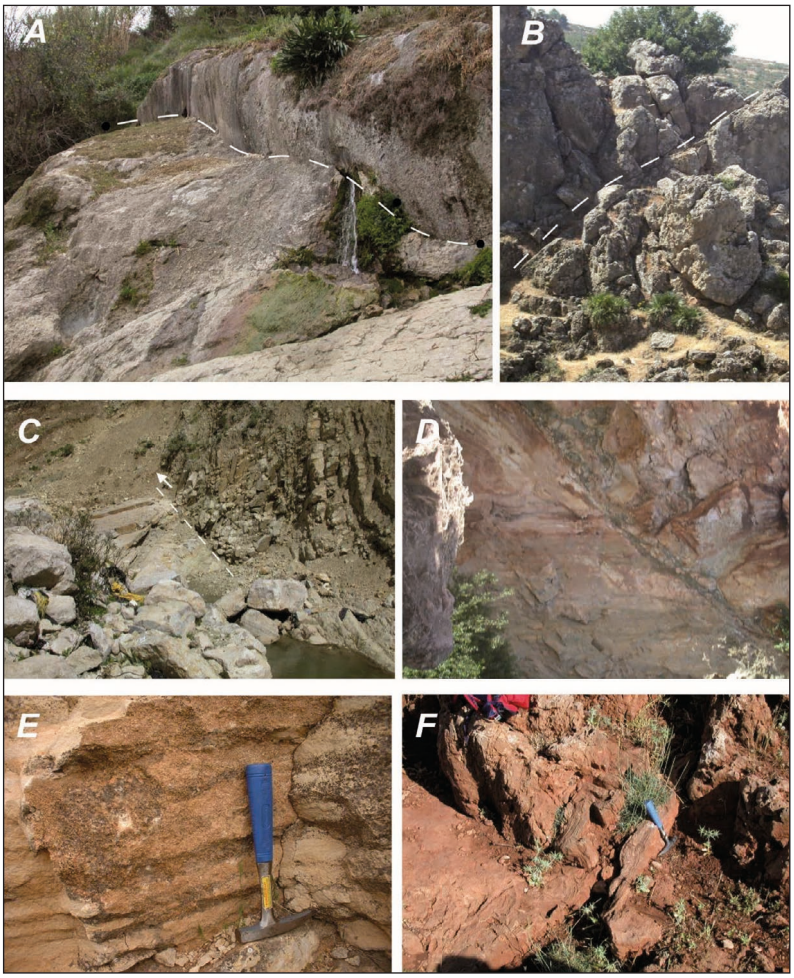

Fig. 13. The brittle structures of the South Rifain Ridges to the north of Meknes; (a) reverse fault in the Jurassic limestone on the northern flank of Kannoufa, forming a water executor, (b) reverse fault in the Jurassic limestones of Zerhoun, (c, d) Northward backlimb thrust, respectively, at the front of the My Idriss ridge (executor of the Aïn Hamma thermal spring) and at the front of Jb. Zerhoun, (e–f) NE-SW dextral strike-slip faults are marked by striations (My Idriss limestones) (e) or calcite (Jb. Kannoufa) (f)

terrains. These faults show a normal displacement of up to several tens of metres at the level of the corridors; in other places, their displacements are decimetric and rarely metric.

A strong basis of prior research as well as structural and geodynamic investigations carried out in the area, especially those done by [Faugères, 1978; Haddaoui et al.,1997 and Chalouan et al., 2014] are necessary for the analysis and interpretation of these data. The geodynamic evolution of the South rifain ridges appears to be within the structural context of the Alpine orogeny, specifically in relation to the convergence of the Africa-Alboran and Eurasia plates in the western Mediterranean region, according to the work of researchers [Anderieux et al., 1971; Anderieux and Mattauer, 1973; Durant Delga and Fontbote, 1980; Hervouet, 1985; El Hatimi, 1991, and Haddaoui et al., 1997]. More specifically, [Haddaoui et al.,1997] proposed a relationship between the east-west (E-W) orientation linked to the period of extension that began in the Triassic period, marked by basin-edge faults, and the compressive deformation during the Upper Miocene. At Jbel Zerhoun (north of Meknès), the structure of the ridge corresponds to Jurassic terrain surrounded by marl as presented by [Faugères, 1978], constituted of Toarcian, Bajocian, and Aalenian terrain. This anticlinal structure is complicated by two branches of thrust faults in a northern direction, the most is the one passing through Aïn Hamma (the thermal spring), oriented N70°E and plunging 70° to the south (Fig. 12a, 12b and 12c). At the front of the ridge, a multitude of sub-equatorial reverse faults develop at the mesostructural scale (Fig. 12d, 12e and 12f). The general structure of the sector is dominated by tangential tectonics with a southern vergence; these two branches correspond to backlimb thrusts.

At Jbel Kefs, the general structure is a south-turned anticline, the northern flank consisting of a monoclinal Jurassic series with a relatively shallow dip to the NNE (30° to 40°). This

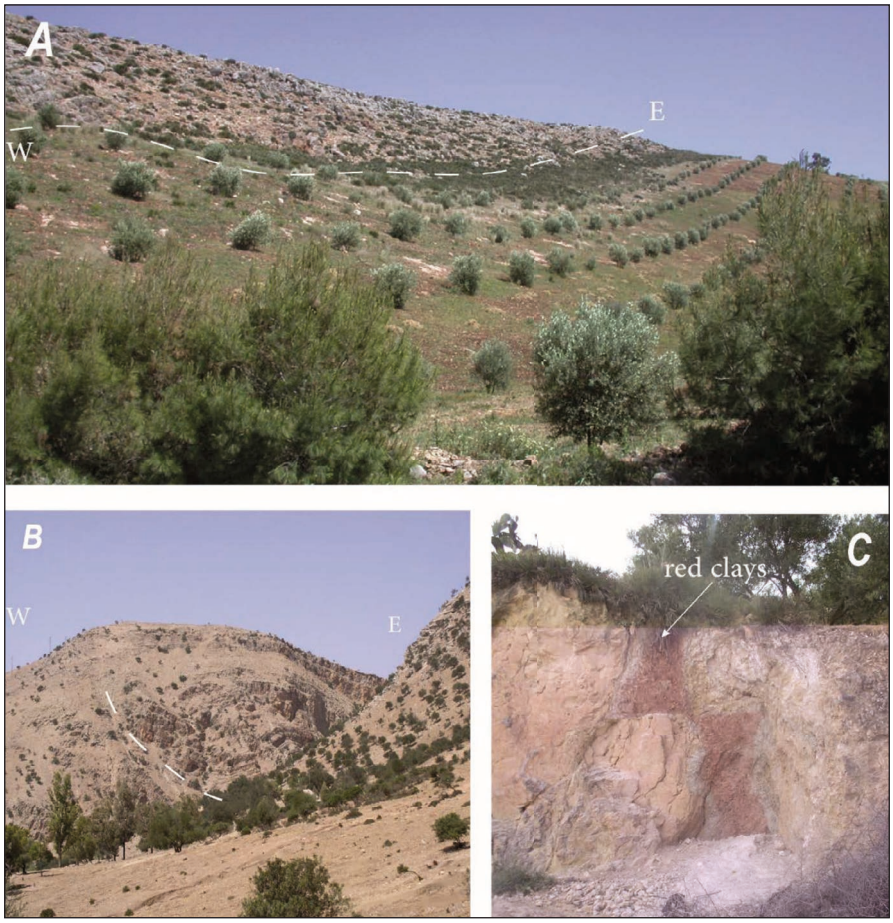

Fig. 14. Structures of the south rifain ridges of Jbel Kefs and Jbel El Kansera; (a) border thrust fault limiting the Jbel Kefs anticline and the Meknes plateau, (b) N-S thrust fault clearly visible of the cluse El Kansera, where the Jurassic series is in subvertical contact with the Upper Miocene marls, (c) boundary fault injected by red clays

anticline is bounded to the south by a major N80 to N110 fault filled by Triassic red clays (Fig. 13a and 13c). The EL Kansera ridge is an approximately meridional structure whose terrain dips regularly to the east (Fig. 13b). It is limited to the west by a clearly visible N-S thrust fault, where the Jurassic series is in subvertical contact with the Upper Miocene marls.

CONCLUSIONS

The objective of this study is to map the directions of major structures in the South Rifain ridges using Landsat-8 OLI images. The lineament map of this region is the result of several Landsat-8 OLI image processing operations and correlations with work in the region. The lineament map shows four main directions: E-W, N-S, NW-SE, and NE-SW. The geometry of the structures is guided by major tangential tectonics with a meridional vergence, responsible for the surrection of the Jurassic reliefs. In the south, the Meknes plain forms part of the large Saïss basin, where the Neogene and Plio-Quaternary terrain, which is relatively less deformed, is subhorizontal, except at the approach to the contact with the Jurassic outcrops of the SRR, where it is significantly deformed.

In general, the structure is dominated by thrust faults, most of which are emergent. The dominant south aspect of the vergence of these tangential tectonics is dampened by large, kilometre-long anticlinal structures, generally oriented E-W, which delimit less deformed synclinal zones. These frontal flexures and the thrust tectonics functioned in conjunction as two manifestations of the same horizontal N-S compressional deformation The association of these structures with a system of dextral NW-SE and sinistral NE-SW conjugate strike-slip faults and normal-component N-S to NNE-SSW faults is integrate in the southward propagation towards to south of deformation in foreland fold and thrust rifian belt.

REFERENCES

1. Abrams, M. J., Brown, D., Lepley, L., Sadowski, R. 1983. Remote sensing for porphyry copper deposits in southern Arizona. Economic Geology, 78(4), 591–604.
2. Adiri, Z., El Harti, A., Jellouli, A., Lhissou, R., Maacha, L., Azmi, M., Zouhair, M., Bachaoui, E.M. 2017. Comparison of Landsat-8, ASTER and Sentinel 1 satellite remote sensing data in automatic lineaments extraction: A case study of Sidi Flah-Bouskour inlier, Moroccan Anti Atlas. Advances in Space Research, 60, 2355–2367. https://doi.org/10.1016/j.asr.2017.09.006
3. Ahmadi, H., Pekkan, E., Seyitoğlu, G. 2023. Automatic lineaments detection using radar and optical data with an emphasis on geologic and tectonic implications: a case study of Kabul Block, eastern Afghanistan. Geocarto International, 38, 2231400. https://doi.org/10.1080/10106049.2023.2231400
4. Ahmed Ii, J.B., Mansor, S. 2018. Overview of the application of geospatial technology to groundwater potential mapping in Nigeria. Arab J Geosci, 11, 504. https://doi.org/10.1007/s12517-018-3852-4
5. Ait Brahim, L., Chotin, Pierre. 1984. Mise en evidence d'un changement de direction de compression dans l'avant-pays rifain (Maroc) au cours du Tertiaire et du Quaternaire. Bulletin de la Société géologique de France, 7(4), 681–691.
6. Ali, A.S., Pour, A.B. 2014. Lithological mapping and hydrothermal alteration using Landsat 8 data: a case study in ariab mining district, red sea hills, Sudan. International Journal of Basic and Applied Sciences, 3(3), 199. https://doi.org/10.14419/ijbas.v3i3.2821
7. Amer, R., Kusky, T., Ghulam, A. 2010. Lithological mapping in the Central Eastern Desert of Egypt using ASTER data. Journal of African Earth Sciences, 56(2–3), 75–82. https://doi.org/10.1016/j.jafrearsci.2009.06.004
8. Amine, A., El Ouardi, H., Zebari, M., El Makrini, H. 2020. Active tectonics in the Moulay Idriss Massif (South Rifian Ridges, NW Morocco): New insights from geomorphic indices and drainage pattern analysis. Journal of African Earth Sciences, 167, 103833. https://doi.org/10.1016/j.jafrearsci.2020.103833
9. Anderson, R.G., Jin, Y., Goulden, M.L. 2012. Assessing regional evapotranspiration and water balance across a Mediterranean montane climate gradient. Agricultural and Forest Meteorology, 166–167, 10–22. https://doi.org/10.1016/j.agrformet.2012.07.004
10. Andrieux, J., and Mattauer, M. 1973. Précisions sur un modèle explicatif de l'Arc de Gibraltar. Bulletin de la Societé Géologique de France, 7(2), 115–118. https://doi.org/10.2113/gssgfbull.S7-XV.2.115
11. Andrieux, J., Fontbote, J. M., Mattauer, M. 1971. Sur un modèle explicatif de l'Arc de Gibraltar. Earth and Planetary Science Letters, 12(2), 191–198. https://doi.org/10.1016/0012-821X(71)90077-X
12. Bargach, K., Ruano, P., Chabli, A. et al. 2004. Recent Tectonic Deformations and Stresses in the Frontal Part of the Rif Cordillera and the Saïss Basin (Fes and Rabat Regions, Morocco). Pure appl.

Geophys, 161, 521–540.

13. Benaissi, L., Tarek, A., Tobi, A., Ibouh, H., Zaid, K., Elamari, K., Hibti, M. 2022. Geological mapping and mining prospecting in the Aouli inlier (Eastern Meseta, Morocco) based on remote sensing and geographic information systems (GIS). China Geology, 5(4), 614–625.
14. Chalouan, A., Galindo-Zaldívar, J, Bargach, K., Ruano-Roca, P, Akil, M., Chabli, A., Jabaloy-Sánchez, A, Ahmamou, A., Sanz De Galdeano, Carlos. 2003. Evolution tectonique du front de la chaîne du Rif et de son avant-pays meseto-atlasique dans un modèle de coin expulsé vers le SW. Third regional commitee atlantic neogene stratigtraphy congress. The atlantic Neogene in the XXI century: state of the art, 45–46
15. Chalouan, A., Gil, A.J., Galindo-Zaldívar, J., Ahmamou, M., Ruano, P., de Lacy, M.C., Ruiz-Armenteros, A.M., Benmakhlouf, M., Riguzzi, F. 2014. Active faulting in the frontal Rif Cordillera (Fes region, Morocco): Constraints from GPS data. SI : Geodynamic Evolution of the Alboran Domain, 77, 110–122. https://doi.org/10.1016/j.jog.2014.01.002
16. Chavez, P.S. 1988. An improved dark-object subtraction technique for atmospheric scattering correction of multispectral data. Remote Sensing of Environment, 24, 459–479. https://doi.org/10.1016/0034-4257(88)90019-3
17. Dang, Y.N., Xiao, L., Xu, Y., Zhang, F., Huang, J., Wang, J., Zhao, J.N., Komatsu, G., Yue, Z. 2018. The Polygonal Surface Structures in the Dalangtan Playa, Qaidam Basin, NW China: Controlling Factors for Their Formation and Implications for Analogous Martian Landforms. JGR Planets, 123, 1910–1933. https://doi.org/10.1029/2018JE005525
18. Das, S., Vincent, J.R. 2009. Mangroves protected villages and reduced death toll during Indian super cyclone. Gretchen C. Daily, Stanford University, Stanford, 106(18), 7357–7360. https://doi.org/10.1073/pnas.0810440106
19. Doski, J.A.H. 2019. Tectonic Analysis of Lineaments in the Gara Anticline, Kurdistan, Northern Iraq. J Indian Soc Remote Sens, 47, 941–950. https://doi.org/10.1007/s12524-019-00940-8
20. Durand-Delga, M., Fontboté, J. M. 1980. Le cadre structural de la Méditerranée occidentale. XXVIth Intern. Geological Congress. Colloque C5: Géologie des chaînes alpines issues de la téthys. Mém. Bur. Rech. Géol. Min., Orléans, 11, 65–85.
21. Chaves, M., Picoli C.A., Sanches, I. 2020. Recent Applications of Landsat 8/OLI and Sentinel-2/MSI for Land Use and Land Cover Mapping: A Systematic Review. Remote Sensing, 12, 3062. https://doi.org/10.3390/rs12183062
22. El Asmi, H., Gourari, L., Benabbou, M., el Yakouti, I., Hayati, A., Chellai, E. H., Theilen-Willige, B. 2023a. Facies architecture of the Plio-Quaternary alluvial fan deposits from south-eastern margin of the Saïss foreland basin (Morocco): Paleoclimatic and neotectonic implications. Journal of African Earth Sciences, 199. https://doi.org/10.1016/j.jafrearsci.2022.104818
23. El Asmi, H., Gourari, L., Benabbou, M., el Yakouti, I., Hayati, A., Azennoud, K., Brahim, Y. A., Chellai, E.H. 2023b. Primary and secondary sedimentary processes in debris-flow-dominated alluvial fan deposits within karstic setting: An example from the Middle Atlas-Sais foreland basin transition zone, Morocco. Journal of African Earth Sciences, 206. https://doi.org/10.1016/j.jafrearsci.2023.105028
24. El Hafyani, M., Essahlaoui, N., Essahlaoui, A., Mohajane, M., van Rompaey, A. 2023. Generation of climate change scenarios for rainfall and temperature using SDSM in a Mediterranean environment: a case study of Boufakrane river watershed, Morocco. Journal of Umm Al-Qura University for Applied Sciences, 9(4), 436–448. https://doi.org/10.1007/s43994-023-00052-7
25. El Hatimi, N., Duee, G., Hervouet, Y. 1991. La Dorsale calcaire du Haouz ; ancienne marge continentale passive tethysienne (Rif, Maroc). Bulletin de la Société géologique de France, 162(1), 79–90. https://doi.org/10.2113/gssgfbull.162.1.79
26. El Yakouti, I., el Asmi, H., Gourari, L., Benabbou, M., Hayati, A., Salah, M., Chellai, E. H. 2024. Facies analysis, architectural elements, and paleoenvironmental reconstruction of alluvial deposits of the low terraces and floodplains in the Middle Sebou river (Eastern Saïss foreland basin, Morocco). Journal of African Earth Sciences, 211. https://doi.org/10.1016/j.jafrearsci.2024.105170
27. Faugères, J.C. 1978. Les Rides sud-rifaines: Evolution sédimentaire et structurale d'un bassin atlantico-mesogéen de la marge africaine. Bordeaux, France: Univ. Bordeaux
28. Fossi, D.H., Djomo, H.D., Takodjou Wambo, J. D., Kouayep Tchoundi, L.C., Deassou Sezine, E., Takam Tchoupe, G.B., Tchatchueng, R. 2021. Extraction and analysis of structural lineaments from Mokolo area, North Cameroon, using DEM and remote sensing images, and their influence on drainage morphometric. Arabian Journal of Geosciences, 14, 1–14. https://doi.org/10.1007/s12517-021-08460-x
29. Frizon de Lamotte, D., Zizi, M., Missenard, Y., Hafid, M., Azzouzi, M. E., Maury, R. C., Michard, A. 2008. The atlas system. Continental Evolution: The Geology of Morocco: Structure, Stratigraphy, and Tectonics of the Africa-Atlantic-Mediterranean Triple Junction, 133–202.
30. Haddaoui, Z., El Hatimi, N., Hervouët, Y. 1997. Les Rides sud-rifaines (Maroc-septentrional) : influence de la géométrie d'un bassin jurassique sur la propagation des chevauchements néogènes. Géologie

Méditerranéenne, 24(1), 51–71.

31. Hamidi, M., Bouramtane, T., Abraham, S., Kacimi, I., Barbiero, L., Kassou, N. ... Levy, G. 2023. Landslide Hazard Assessment in the Heterogeneous Geomorphological and Environmental Context of the Rif Region, Morocco – A Machine Learning Approach. Ecological Engineering & Environmental Technology, 24(8), 272–292. https://doi.org/10.12912/27197050/172569
32. Harris, J. R., Rogge, D., Hitchcock, R., Ijewliw, O., Wright, D. 2005. Mapping lithology in Canada's Arctic: application of hyperspectral data using the minimum noise fraction transformation and matched filtering. Canadian Journal of Earth Sciences, 42(12), 2173–2193. https://doi.org/10.1139/e05-064
33. Hervouet, Y. 1985. Evolution tectono-sédimentaire de l'avant-fosse rifaine du Maroc oriental au Miocène. Bulletin de l'Institut Scientifique (Rabat), 9, 81–88.
34. Islam, M. T., Hasib, K. M., Rahman, M. M., Tusher, A. N., Alam, M. S., Islam, M. R. 2023. Convolutional auto-encoder and independent component analysis based automatic place recognition for moving robot in invariant season condition. Human-Centric Intelligent Systems, 3(1), 13–24. https://doi.org/10.1007/s44230-022-00013-z
35. Jellouli, A., El Harti, A., Adiri, Z., Chakouri, M., El Hachimi, J., Bachaoui, E.M. 2021. Application of optical and radar satellite images for mapping tectonic lineaments in kerdous inlier of the Anti-Atlas belt, Morocco. Remote Sensing Applications: Society and Environment, 22, 100509. https://doi.org/10.1016/j.rsase.2021.100509
36. Khan, M.Y.A., ElKashouty, M., Subyani, A. M., Tian, F. 2023. Morphometric determination and digital geological mapping by RS and GIS Techniques in Aseer–Jazan Contact, Southwest Saudi Arabia. Water, 15(13), 2438. https://doi.org/10.3390/w15132438
37. Lathrop Jr, R. G., Lillesand, T. M. 1987. Calibration of thematic mapper thermal data for water surface temperature mapping: case study on the Great Lakes. Remote Sensing of Environment, 22(2), 297–3 https://doi.org/10.1016/0034-4257(87)90063-0
38. Mahan, A., Arfania, R. 2018. Exploring porphyry copper deposits in the central Iran using remote sensing techniques. Open Journal of Geology, 8(6), 606. https://doi.org/10.4236/ojg.2018.86035
39. Mamouch, Y., Attou, A., Miftah, A., Ouchchen, M., Dadi, B., Achkouch, L., Et-tayea, Y., Allaoui, A., Boualoul, M., Randazzo, G., Lanza, S., Muzirafuti, A. 2022. Mapping of Hydrothermal Alteration Zones in the Kelâat M'Gouna Region Using Airborne Gamma-Ray Spectrometry and Remote Sensing Data: Mining Implications (Eastern Anti-Atlas, Morocco). Applied Sciences, 12, 957. https://doi.org/10.3390/app12030957
40. Mars, J. C., Rowan, L. C. 2010. Spectral assessment of new ASTER SWIR surface reflectance data products for spectroscopic mapping of rocks and minerals. Remote Sensing of Environment, 114(9), 2011–2025. https://doi.org/10.1016/j.rse.2010.04.008
41. Masoud, A., Koike, K. 2006. Tectonic architecture through Landsat-7 ETM+/SRTM DEM-derived lineaments and relationship to the hydrogeologic setting in Siwa region, NW Egypt. Journal of African Earth Sciences, 45, 467–477. https://doi.org/10.1016/j.jafrearsci.2006.04.005
42. Ortiz, J.D., Avouris, D.M., Schiller, S.J., Luvall, J.C., Lekki, J.D., Tokars, R.P., Becker, R. 2019. Evaluating visible derivative spectroscopy by varimax-rotated, principal component analysis of aerial hyperspectral images from the western basin of Lake Erie. Journal of great lakes research, 45(3), 522–535. https://doi.org/10.1016/j.jglr.2019.03.005
43. Pour, A.B., and Hashim, M. 2012. The application of ASTER remote sensing data to porphyry copper and epithermal gold deposits. Ore geology reviews, 44, 1–9. https://doi.org/10.1016/j.oregeorev.2011.09.009
44. Preeja K. R., Joseph, S., Thomas, J., Vijith H. 2011. Identification of groundwater potential zones of a tropical river basin (Kerala, India) Using Remote Sensing and GIS Techniques. J Indian Soc Remote Sens, 39, 83–94. https://doi.org/10.1007/s12524-011-0075-5
45. Sani, F., Del Ventisette, C., Montanari, D., Bendkik, A., Chenakeb, M. 2007. Structural evolution of the Rides Prerifaines (Morocco): structural and seismic interpretation and analogue modelling experiments. International Journal of Earth Sciences, 96(4), 685–706. https://doi.org/10.1007/s00531-006-0118-2
46. Sassioui, S., Lakhloufi, A., Aarab, A., Zouggarh, A., El Hilali, M., Courba, S., Larabi, A. 2023. Contribution of remote sensing to the mapping of lineaments and ore-mineral occurrences in the Taghbalt Region, Moroccan Eastern Anti-Atlas. The Iraqi Geological Journal, 307–323. https://doi.org/10.46717/igj.56.2D.23ms-2023-10-29
47. Si Mhamdi, H., Raji, M., Maimouni, S., Oukassou, M. 2017. Fractures network mapping using remote sensing in the Paleozoic massif of Tichka (Western High Atlas, Morocco). Arab J Geosci, 10, 125. https://doi.org/10.1007/s12517-017-2912-5
48. Stead, D., Donati, D., Wolter, A., Sturzenegger, M. 2019. Application of Remote Sensing to the Investigation of Rock Slopes: Experience Gained and Lessons Learned. IJGI, 8, 296. https://doi.org/10.3390/ijgi8070296
49. Taj, B., Mastere, M., Benzougagh, B., El Hilali, M., Sassioui, S., El Fellah, B. 2024. Geotechnical Prospects and Electrical Tomography to Study Slope Instability

in the Rif Alboran Sea Shoreline on the Mediterranean By-Road (Northern Morocco). Ecological Engineering & Environmental Technology (EEET), 25(1).

50. Yousefi, T., Aliyari, F., Abedini, A., Calagari, A.A. 2018. Integrating geologic and Landsat-8 and ASTER remote sensing data for gold exploration: a case study from Zarshuran Carlin-type gold deposit, NW Iran. Arabian Journal of Geosciences, 11, 1–19. https://doi.org/10.1007/s12517-018-3822-x
51. Zafaty, O., Oukassou, M., Si Mhamdi, H., Tabuce, R., Charrière, A. 2023. Integrated remote sensing data and field investigations for geological mapping and structural analysis. The case of SW Tichoukt ridge (Middle Atlas, Morocco). Journal of African Earth Sciences, 198, 104784. https://doi.org/10.1016/j.jafrearsci.2022.104784
52. Zizi, M. 2002. Triassic-Jurassic extensional systems and their Neogene reactivation in northern Morocco (the Rides Prerifaines and Guercif Basin). Notes Mem. Serv. Geol. Maroc, 146, 1–138.